

RESEARCH

Open Access



Nanoparticle delivery of si-Notch1 modulates metabolic reprogramming to affect 5-FU resistance and cell pyroptosis in colorectal cancer

Dan-dan Li^{1†}, Jia-cheng Jin^{2†}, Xuan-wen Liu³, Shu-yang Liu⁴, Fu-jian Ji⁴ and Tong Liu^{4*}

[†]Dan-dan Li and Jia-cheng Jin contributed equally to this study.

*Correspondence: atong@jlu.edu.cn

¹ Department of Gastrointestinal Medicine (Endoscopy Center), China-Japan Union Hospital of Jilin University, Changchun 130033, China

² Department of Urinary Surgery, First Hospital of Dalian Medical University, Dalian 116011, China

³ Department of Gastrointestinal Surgery, Jilin Central Hospital, Jilin 132000, China

⁴ Department of Gastrointestinal Colorectal Surgery, China-Japan Union Hospital of Jilin University, No. 126 XianTai Street, Changchun 130033, China

Abstract

Background: Nanocarrier delivery of small interfering RNAs (siRNAs) to silence cancer-associated genes is a promising method for cancer treatment. Here, we explored the role and mechanisms of PLAG NPs-delivered si-Notch1 in colorectal cancer (CRC).

Results: High Notch1 expression was observed in both sensitive and resistant CRC tissues and cells. Notch1 silencing repressed proliferation and facilitates apoptosis of resistant CRC cells, and suppressed glycolysis and promoted pyroptosis in resistant CRC cells. Notch1 directly interacts with PCAF. Notch1 knockdown's suppressive effect on glycolysis was reversed by overexpression of PCAF. Moreover, a nanocarrier called PLAG NPs was built with a higher delivery efficiency compared with lipo2000. Si-Notch1 delivered by PLAG NPs efficiently overcame the CRC cells' 5-FU resistance and facilitated pyroptosis in a CRC mouse model.

Conclusions: PLAG NPs carrying si-Notch1 had a great advantage in the extension of half-life circulation and targeting ability, providing a theoretical foundation for precise clinical treatment of CRC.

Keywords: Colorectal cancer, PLGA NPs, Notch1, Resistance, Glycolysis, Pyroptosis

Background

Colorectal cancer (CRC) is the second leading cause of death related to cancer globally (Hagan et al. 2013; Bray et al. 2018). By 2030, 2.2 million new CRC cases will be reported, and 1.1 million people will die (Arnold et al. 2017). Currently, the major methods for CRC treatment are chemotherapy, surgery, radiotherapy, targeted therapy, and so on (Billir and Schrag 2021). The 5-fluorouracil-based (5-FU) chemotherapy remains the cornerstone of CRC therapy. However, its clinical effectiveness is limited by antimicrobial resistance (Grothey et al. 2018; Zhang et al. 2008). Therefore, it is of great concern to identify novel targets to improve CRC chemotherapy.

Metabolic reprogramming is an important hallmark of tumor cells (DeBerardinis et al. 2008; Pavlova and Thompson 2016), which is characterized by a weakened



OXPHOS system with energy compensation via the pentose phosphate pathway (PPP) or glycolysis (DeBerardinis and Chandel 2016; Kim et al. 2020). As the classic pathway for producing energy, glycolysis allows cancer cells to generate energy in the presence of oxygen (Diaz-Ruiz et al. 2011). More importantly, convincing evidence has shown that glycolysis suppression increases drug sensitivity and pyroptosis of cancer cells (Bhattacharya et al. 2016; Hay 2016; Li et al. 2021; Su et al. 2023). Pyroptosis, a form of pro-inflammatory programmed cell death, is involved in proliferation, invasion, and metastasis of tumor cells (Fang et al. 2020; Yang et al. 2022). Thus, targeting glycolysis is a treatment alternative to strengthen drug susceptibility and regulate pyroptosis of cancer cells.

Notch, an ancient signaling pathway in mammals, contains four Notch receptors (Notch 1–4) (Leong and Gao 2008; Nicolas et al. 2003). The Notch pathway is activated when Notch receptors interact with ligands (Bigas et al. 1998). Compared to other Notch receptors, Notch1 is responsible for CRC progression (Tyagi et al. 2020; Vinson et al. 2016). For example, down-regulation of Notch1 impairs proliferation of CRC cells (Wang et al. 2022). POFUT1 knockdown contributes to CRC cell apoptosis via Notch1 down-regulation (Du et al. 2018). MiR-744 up-regulation evidently represses proliferation and invasion of CRC cells by down-regulating Notch1 (Shen and Li 2018). Notch1 promotes glycolysis in lung cancer, suggesting that Notch1 is an important transcription factor that regulate glycolysis (Xie et al. 2021). However, the effect of Notch1 on glycolysis in CRC remains unclear.

As we all know, small interfering RNAs (siRNAs) are able to silence cancer-related genes, reducing levels of their target genes (Davidson and McCray 2011; Kanasty et al. 2012). Nevertheless, naked siRNAs have a short half-life and it is difficult to reach the target sites (Singh et al. 2018; Setten et al. 2019). Thus, proper delivery systems are needed to protect siRNAs from degradation and transport siRNAs to target sites. PLGA NPs (poly lactic-co-glycolic acid nanoparticles) are carriers that deliver biological molecules, peptides, and chemotherapeutic drugs (Firouzi-Amandi et al. 2018; Najahi-Missaoui et al. 2020). PLGA NPs can enter cells, prolonging the half-life of their cargo and improving the efficiency of drug use (Cartiera et al. 2009; Sadat Tabatabaei Mirakabad et al. 2014). PLGA NPs have been used to deliver siRNAs to cancers (Ghareghomi et al. 2021; Mohammad Gholinia Sarpoli et al. 2022; Pho-Iam et al. 2021). However, there are few studies on PLGA NPs carrying si-Notch1 for CRC treatment.

It is previously reported that Notch1-induced transcription of glycolytic genes is mainly mediated via p300/CBP-associated factor (PCAF) and histone acetyltransferases p300 (Wallberg et al. 2002; Thorne et al. 2009). PCAF interacts with hypoxia-inducible factor 1 α (HIF-1 α) to regulate glycolytic production and apoptosis (Rajendran et al. 2013; Xenaki et al. 2008). Under anoxic conditions, HIF-1 α enhances glycolysis and promotes tumor progression (Semenza 2002, 2003), which up-regulates membrane transporters and glycolytic enzymes to increase glucose flux (Zhao et al. 2020; Wang et al. 2014). In particular, HIF-1 α induces glycolysis to impart 5-FU resistance (Dong et al. 2022). Therefore, it is worth investigating whether Notch1 modulates glycolysis to affect 5-FU resistance by regulating the PCAF/HIF-1 α axis in CRC.

In this study, we explored the function of si-Notch1 delivered by PLGA NPs in CRC and investigated the underlying mechanism.

Methods

Cell culture

The human CRC cell lines (HCT8 and SW620) were purchased from the Cell Bank of the Chinese Academy of Sciences (Shanghai, China). These cells were then cultured in RPMI 1640 medium (Gibco, Billings, MT, USA) supplemented with 10% fetal bovine serum (FBS) and 1% penicillin–streptomycin, which were incubated at 37 °C in a humidified incubator with 5% CO₂. All cells were tested using a Mycoplasma Stain Assay Kit (Beyotime, Shanghai, China).

And 5-FU resistant cell lines (SW620-R and HCT8-R) were established using the following method. We treated SW620 and HCT8 cells with increasing concentrations of 5-FU dissolved in physiological saline (10⁻⁸–10⁻⁴ M). 5-FU resistance was assessed by calculating the half-maximal inhibitory concentration (IC₅₀). 5-FU resistance was defined as a resistance index (RI, IC₅₀ of the WT cells/IC₅₀ of the 5-FU-R cells) > 10 after treatment with 5-FU for 8 months.

Cell transfection

We bought si-Notch1, si-NC (negative control), pcDNA3.1-NC, and pcDNA3.1-Notch1 from RiboBio (Guangzhou, China). We transfected the above plasmids into SW620-R, HCT8-R, SW620 and HCT8 cells via Lipofectamine 2000 (lipo2000; Invitrogen, Carlsbad, CA, USA) for 48 h.

Cell Counting Kit-8 (CCK-8) assay

To calculate the IC₅₀ value, HCT8, HCT8-R, SW620, and SW620-R cells were seeded in 96-well plates at 5 × 10³/well and then incubated with 0.1, 1, 10, 100, and 500 μM 5-FU for 2 d. Next, 10 μL CCK-8 solution (Sevenbio, Beijing, China) was added and further incubated for 3 h at 37 °C. The optical density at 450 nm (OD₄₅₀) was measured using a Bio-Tek MQX200 microplate reader (BioTek, Winooski, VT, USA). GraphPad Prism software (version 5.0) was used to calculate the IC₅₀ values.

The OD₄₅₀ was measured at 24, 48, and 72 h after treatment with 5-FU (5 μg/mL) to examine cell viability. The remaining procedures were performed as previously described.

Clinical samples

CRC and adjacent normal tissues (*n* = 50 pairs) were obtained from sensitive (*n* = 33) and resistant (*n* = 17) CRC patients who underwent surgery between January 2020 and May 2022. Two independent pathologists examined the patients' histopathological features. The clinical characteristics of the patients are presented (Additional file 1: Table S1). We assigned all CRC patients to Notch1 high- or low-expression groups based on Notch1 expression's median value in tumor tissues. Written informed consent was obtained from all the enrolled patients. This study was approved by the Ethics Committee of the China-Japan Union Hospital of Jilin University (2023-KYYS-021) and conformed to the Declaration of Helsinki.

qRT-PCR

Total RNA was extracted from CRC cells using TRIzol reagent (Invitrogen) and then measured through a NanoDrop spectrophotometer (NanoDrop Technologies, USA). In accordance with the instructions of the Reverse Transcription Kit (Takara, Dalian, China), complementary DNA for Notch1 was synthesized. Then qRT-PCR was performed using the SYBR Premix Ex Taq™ II kit (Takara). The following primers were used: Notch1 (F: 5'-GCAGTTGTGCTCCTGAAGAA-3'; R: 5'-CGGGCGGCCAGAAC-3') and GAPDH (F: 5'-AAGGTGAAGGTCGGAGTCAAC-3'; R: 5'-GGGGTCATTGATGGCAACAATA-3'). Thermal cycling was performed as follows: 95 °C for 5 min, followed by 40 cycles at 95 °C for 15 s, 62 °C for 1 min, and 70 °C for 15 s. Relative expression of Notch1 was calculated using the $2^{-\Delta\Delta Ct}$ method, which was normalized to GAPDH.

Flow cytometry analysis

An Annexin V-propidium iodide (PI) kit (Invitrogen) was used to evaluate cell apoptosis. Based on instructions of this kit, cells (3×10^5 per well) were suspended in a binding buffer, followed by staining with 5 μ L Annexin V-FITC for 15 min and 5 μ L PI solution for 5 min under darkness. The stained cells were analyzed using flow cytometry. Apoptotic rate was calculated as the percentage of early and late apoptotic cells.

Co-immunoprecipitation (IP) analysis

SW620-R cells were lysed with IP lysis buffer (30 mM Tris, 150 mM NaCl, 1% Triton X-100, 10% glycerol, 100 μ M orthovanadate, 0.5 mM EDTA, 10 mM NaF, 200 μ M PMSF; pH 7.5) with phosphatase and protease inhibitors. Next, anti-Notch1 (ab52627, Abcam, Cambridge, CA, USA) or anti-PCAF (ab176316, Abcam) were added and incubated with cell lysates overnight, followed by incubation with magnetic protein A/G beads (Pierce, Rockford, IL, USA) at 4 °C for 2 h. Finally, the immune complexes were washed with PBS and analyzed by western blotting.

Western blot

The cells or tissues were dissolved in RIPA buffer (Beyotime). Proteins (50 ng) were separated by SDS polyacrylamide gel electrophoresis (10%) and transferred to PVDF membranes. After blocking with 5% non-fat milk for 15 min, the membranes were incubated with primary antibodies (Abcam, Cambridge, CA, USA) overnight at 4 °C. The primary antibodies used were anti-Notch1 (1:2000; ab52627), anti-Bax (1:2000; ab52627), anti-cleaved caspase-3 (1:500; ab32042), anti-Bcl-2 (1:1000; ab32124), anti-p53 (1:2000; ab32049), anti-PCAF (1:1000; ab176316), anti-HIF-1 α (1:1000; ab179483), anti-GLUT3 (1:1000; ab15311), anti-LDHA (1:5000; ab52488), anti-PKM2 (1:2000; ab85555), anti-PGK1 (1:2000; ab199438), anti-HK2 (1:1000; ab209847), anti-GLUT1 (1:2000; ab115730), anti-ALDOA (1:1000; ab252953), anti-NLRP3 (1:1000; ab263899), anti-caspase-1 (1:1000; ab207802), anti-GSDMD-N (1:1000; ab215203), anti-IL-18 (1:1000; ab243091), anti-IL-1 β (1:1000; ab254360) and anti- β -actin (1:1000; ab8227). The membranes were then incubated with anti-rabbit secondary antibody (1:2000, ab6721) for 2 h. The protein bands were detected using an ECL substrate reaction kit. ImageJ software (NIH, USA) was used to quantify protein band intensity.

Immunofluorescence

SW620-R and HCT8-R cells were fixed (4%) for 20 min and permeabilized with Triton X-100 (0.25%) for 5 min. Subsequently, the cells were blocked with 10% goat serum for an hour and incubated with the primary antibody anti-Notch1 (1:150, ab52627, Abcam). The next day, anti-rabbit secondary antibody (1:500, ab150077, Abcam) was added and incubated for 1 h. We added DAPI for staining nucleic acids, and images were captured using a Nikon ECLIPSE E800 fluorescence microscope.

Immunohistochemistry (IHC) staining

IHC staining was performed to examine protein expression levels of Notch1, PCAF, and HIF-1 α . Tissue samples were fixed with 10% formalin, embedded in paraffin, and sliced into sections (4- μ m). Subsequently, they were dewaxed using xylene and rehydrated using alcohol. After antigen repair and blocking of nonspecific sites, the sections were incubated with primary antibodies including anti-Notch1 (1:150, ab52627, Abcam), anti-PCAF (1:200, PA5-99179, Invitrogen), and anti-HIF-1 α (1:100, ab51608, Abcam) at 4 °C. The next day, anti-rabbit secondary antibody (1:500, ab6112, Abcam) was added and incubated for half an hour. Then 3,3'-diaminobenzidine substrate solution was added. Finally, the nuclei were stained with hematoxylin and stained areas were observed under a microscope (Olympus, Tokyo, Japan).

Glucose consumption analysis

We used a Glucose Assay Kit to examine the glucose level in the culture medium of CRC cells. Under peroxidase action, hydrogen peroxide could conjugate 4-amino-antipyrine with phenol to synthesize quinones, which were then examined using a spectrophotometer. The glucose level was calculated using the formula: glucose content (mmol/L) = sample tube absorbance value (A)/standard tube absorbance value \times standard concentration (5.55 mmol/L).

Lactate production analysis

A Lactate Assay Kit (Nanjing Jiancheng) was used to assess the lactate level in the culture medium of CRC cells. The principle of lactate determination was that acid dehydrogenase (LDH) catalyzes the dehydrogenation of lactate to pyruvate, which converted NAD⁺ to NADH. Among these compounds, 5-methylphenazinium methosulfate reduced nitrotetrazolium blue chloride to purple compounds, which were determined by spectrophotometry. The lactate level was calculated using the following formula: lactate level (mmol/L) = sample tube absorbance value (A)/standard tube absorbance value \times standard concentration (3 mmol/L).

EDU assay

We conducted EDU assay to evaluate proliferation of SW620-R and HCT8-R cells using a Cell-Light EDU DNA Cell Proliferation Kit (RiboBio). First, we incubated SW620-R and HCT8-R cells with EDU (50 μ M) for 2 h and washed with PBS 2 times. The cells were then fixed with 4% paraformaldehyde, followed by staining with 1 \times Apollo dye solution in the dark. Finally, we added 1 \times Hoechst33342 to each well and incubated for 30 min. A fluorescence microscope was used for microscopic observation.

Preparation of si-Notch1/si-NC-loaded PLGA NPs

The PLGA NPs core was constructed using a previously reported (Luk et al. 2014; Rishayanti et al. 2018). Briefly, PLGA (20 mg) dissolved in acetone was added to deionized water supplemented with si-Notch1 (20 μ M), followed by addition of mixed solution. Next, it was placed in a vacuum drying oven to volatilize the acetone to obtain the NP core. Fluorescently labeled nanoparticles were generated using the aforementioned method with the modification that si-Notch1/si-NC was substituted with fluorescein (FAM)-labeled si-Notch1/si-NC.

Agarose gel electrophoresis

Agarose gels were purchased from HUAQISHENG (Guangzhou, China) and prepared using $1 \times$ Tris–acetate (TAE) buffer (Biosharp, Beijing, China). Samples were electrophoresed at 140 V for 30 min. An ultraviolet gel imaging system (UVP GelStudio PLUS Touch, Germany) was used to examine the bands.

Dynamic light scattering (DLS) analysis

The hydrodynamic diameter of siRNA@PLGA NPs were measured using dynamic light scattering. Briefly, freeze-dried siRNA-loaded PLGA NPs were re-dispersed in deionized water by gentle sonication for 1 m, and then filtered using syringe filter (0.22 μ m). The measurement was performed on the undiluted samples using Zetasizer Nano ZS (Malvern Instrument, US), which was equipped with a 633 nm of laser at a scattering angle of 173°.

Encapsulation efficiency and loading efficiency of PLAG NPs carrying si-NC/si-Notch1

A dispersion of siRNA or PLAG NPs-loaded formulations was separated by ultracentrifuge at 15,000 rpm at 4 °C. Then harvested nanoparticles were incubated with Triton X 100 for 30 min. After that, PLAG NPs or siRNA in the filtrate and broken nanoparticles were measured through NanoDrop (Thermo Fisher, Waltham, MA, USA) and UV/VIS Spectrophotometer (Biochrom, Holliston, MA, USA), respectively. The encapsulation efficiency and loading capacity efficiency were calculated with the following formula: encapsulation efficiency = $[(W_e - W_f)/W_e] \times 100\%$; loading efficiency = $[(W_e - W_f)/W_t] \times 100\%$. W_e is the weight of added siRNA or PLAG NPs, W_f is the weight of siRNA or PLAG NPs in the filtrate, and W_t is the total nanoparticle weight.

Detection of siRNA release

Using Cy5.5-labeled siRNAs@PLGA NPs, release kinetics of si-Notch1/si-NC from PLGA NPs was examined. Cy5.5-si-Notch1/si-NC@PLGA NPs were suspended in PBS buffer, and then a small volume of sample solutions were taken in triplicate at the indicated time points. After the nanoparticles were centrifuged and disintegrated in DMSO, the fluorescence intensity of Cy5.5-si-Notch1/si-NC was measured by Xenogen IVIS Lumina imaging system (Perkin Elmer, Shanghai, China).

Cellular uptake detection of PLGA NPs

SW620-R and HCT8-R cells were seeded into 24-well plates. Following 24 h of incubation, cells were transfected with FAM-labeled PLGA NPs carrying si-Notch1 or

FAM-labeled si-Notch1 using lipo2000. The cells were then washed twice with PBS and fixed with 4% paraformaldehyde for 10 min, followed by nuclear staining. At last, cells were observed under a laser scanning confocal microscope (Carl Zeiss, Oberkochen, Germany).

Nude mice tumorigenesis assay

We obtained mice (to 4- to 5-week-old, Females BALB/c nude mice) from the Vital River Laboratory Animal Technology, China. The mice were kept under controlled conditions (room temperature, 50% humidity, 12 h L/D cycle) and provided free access to food and water. All experiments involving animals were approved by the Institutional Animal Care and Use Committee of the Jilin University (KT202302010). The experimental procedures were performed in accordance with the guidelines of the National Institute of Health.

To induce the xenograft tumor model, each mouse was subcutaneously injected with HCT8-R cells (5×10^6) via the left armpit. From day 7 post-injection, tumor width and diameter were gauged. Tumor volume was calculated according to the formula: volume = $0.5 \times \text{length} \times \text{width}^2$. When the xenograft tumor volume reached 200 mm³, the tumors were injected with PBS, FAM-labeled si-Notch1 only, FAM-labeled PLGA NPs, or FAM-labeled PLGA NPs-si-Notch1. Mice were randomly divided into four groups ($n=3/\text{group}$). Six hours later, the mice were euthanized, and the tumors and organs were isolated. The bio-distribution of si-Notch1 was determined using the Xenogen IVIS Lumina system (IVIS Spectrum, PerkinElmer).

In addition, we injected xenotypic mice with PBS, FAM-labeled si-Notch1 only, FAM-labeled PLGA NPs, or FAM-labeled PLGA NPs-si-Notch1 (half with and half without 5-FU treatment [10 mg/kg, intraperitoneal injection]) once every 3 days through the tail vein. Mice were randomly divided into eight groups ($n=3/\text{group}$). After treatment for 35 days, all mice were euthanized, and tumors were collected. Tumor volume was calculated and tumor weight was measured.

Statistical analysis

Quantitative data were statistically analyzed using the GraphPad Prism 7.0 software (GraphPad, San Diego, CA, USA). Data from at least three independent experiments are presented as mean \pm standard deviation (SD). The Student's t-test was used to compare differences between the two groups. Differences between multiple groups were compared using one-way ANOVA variance followed by Tukey's test. Statistical significance was defined as $P < 0.05$.

Results

Notch1 expression is up-regulated in 5-FU-resistant CRC tissues/cells

First, we constructed two 5-FU resistant cell lines (SW620-R and HCT8-R cells). Data from the CCK-8 assay showed that the addition of 5-FU resulted in lower viability of SW620 and HCT8 cells than that of SW620-R and HCT8-R cells ($P < 0.01$, Fig. 1A). As exhibited in Fig. 1A, the IC₅₀ of 5-FU in four cell lines was IC₅₀ = 4.246 μM for SW620 cells, IC₅₀ = 142.5 μM for SW620-R cells, IC₅₀ = 18.06 μM for HCT8 cells, and IC₅₀ = 376.3 μM for HCT8-R cells. Next, we assessed apoptosis following 5-FU

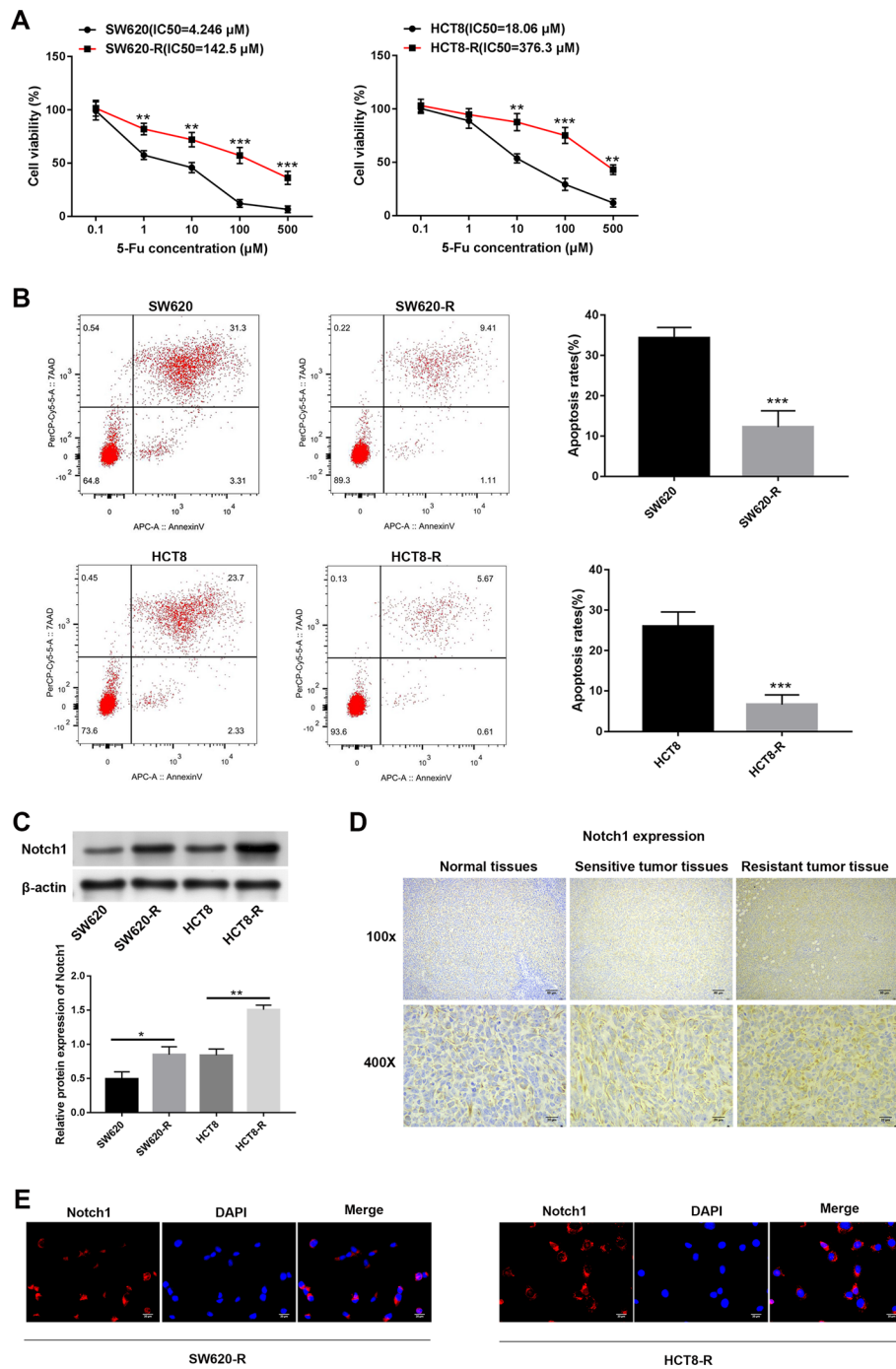


Fig. 1 Notch1 expression is raised in 5-FU-resistant tissues of CRC patients and CRC cell lines. **A** The viability of SW620, SW620-R, HCT8 and HCT8-R cells was detected CCK-8 assay following 5-FU treatment for 48 h. **B** Apoptosis rates of SW620, SW620-R, HCT8 and HCT8-R cells were examined using flow cytometry analysis. **C** Western blot was used to detect protein expression of Notch1 in SW620, SW620-R, HCT8 and HCT8-R cells. **D** Immunohistochemistry staining was used to detect protein expression of Notch1 in normal, sensitive tumor tissues and resistant tumor tissues from CRC patients. **E** Immunofluorescence was used to detect protein expression of Notch1 in SW620-R and HCT8-R cells. * $P < 0.05$. ** $P < 0.01$. *** $P < 0.001$

treatment. We found that SW620-R cells presented a lower apoptosis rate than SW620 cells and HCT8-R cells presented a lower apoptosis rate than HCT8 cells ($P < 0.001$, Fig. 1B).

High expression of Notch1 been observed in CRC. Its high expression is associated with poor prognosis (Additional file 2: Figure S1, Additional file 3: Figure S2, Additional file 4: Figure S3). Therefore, we investigated Notch1 expression in HCT8-R and SW620-R cells. Western blotting showed that Notch1 protein expression in SW620-R/HCT8-R cells was significantly higher than that in SW620/HCT8 cells ($P < 0.05$, Fig. 1C). Tumor tissues from 5-FU resistant patients showed higher protein expression of Notch1 than tumor tissues of 5-FU sensitive patients, and tumor tissues of 5-FU sensitive patients showed higher protein expression of Notch1 than adjacent normal tissues (Fig. 1D). In addition, immunofluorescence was performed to monitor the cell localization of Notch1, which showed that Notch1 was distributed in the cytoplasm of SW620-R and HCT8-R cells (Fig. 1E).

Silencing of Notch1 overcomes 5-FU-induced resistance in CRC cells

To determine the effect of Notch1 on SW620-R and HCT8-R cells, Notch1 was silenced. The silencing efficiency of Notch1 was detected by qRT-PCR, which indicated that Notch1 expression markedly decreased in response to transfection with si-Notch1 ($P < 0.01$, Fig. 2A). Then functional experiments of Notch1 were performed. Based on EDU assay, compared to the si-NC group, silencing of Notch1 dramatically suppressed proliferation of SW620-R and HCT8-R cells ($P < 0.01$, Fig. 2B). Flow cytometry demonstrated that compared to the si-NC group, Notch1 silencing facilitated apoptosis in SW620-R and HCT8-R cells ($P < 0.01$, Fig. 2C). Simultaneously, the expression of apoptosis-related proteins (Bax, cleaved caspase-3, Bcl-2, and p53) was detected using western blotting. Silencing Notch1 reduced the expression level of Bcl-2 and increased expression levels of Bax, cleaved caspase-3, and p53 in SW620-R and HCT8-R cells ($P < 0.05$, Fig. 2D).

In addition, we examined the effect of Notch1 on SW620 and HCT8 cells after treatment with 5-FU for 48 h. Notch1 expression was dramatically increased in SW620 and HCT8 cells after transfection with pcDNA-Notch1 ($P < 0.001$, Fig. 2E). Notch1 overexpression enhanced cell viability and reduced apoptosis in SW620 and HCT8 cells ($P < 0.05$, Fig. 2F, G). Notch1 overexpression led to up-regulation of Bcl-2 expression and down-regulation of Bax, cleaved caspase-3, and p53 expression in SW620 and HCT8 cells ($P < 0.05$, Fig. 2H).

(See figure on next page.)

Fig. 2 Silencing of Notch1 overcomes 5-FU-induced resistance in CRC cells. **A** Relative expression of Notch1 in SW620-R and HCT8-R cells was detected by qRT-PCR after transfection with si-NC or si-Notch1. **B** The proliferation of SW620-R and HCT8-R cells was assessed by EDU assay. **C** Apoptosis rates of SW620-R and HCT8-R cells were examined using flow cytometry analysis. **D** Western blot was used to detect protein expression of Bax, cleaved caspase-3, Bcl-2 and p53 in SW620-R and HCT8-R cells. **E** Relative expression of Notch1 in SW620 and HCT8 cells was detected by qRT-PCR after transfection with pcDNA-NC or pcDNA-Notch1. **F** The viability of SW620 and HCT8 cells was detected CCK-8 assay. **G** Apoptosis rates of SW620 and HCT8 were examined using flow cytometry analysis. **H** Western blot was used to detect protein expression of Bax, cleaved caspase-3, Bcl-2 and p53 in SW620 and HCT8 cells. * $P < 0.05$. ** $P < 0.01$. *** $P < 0.001$

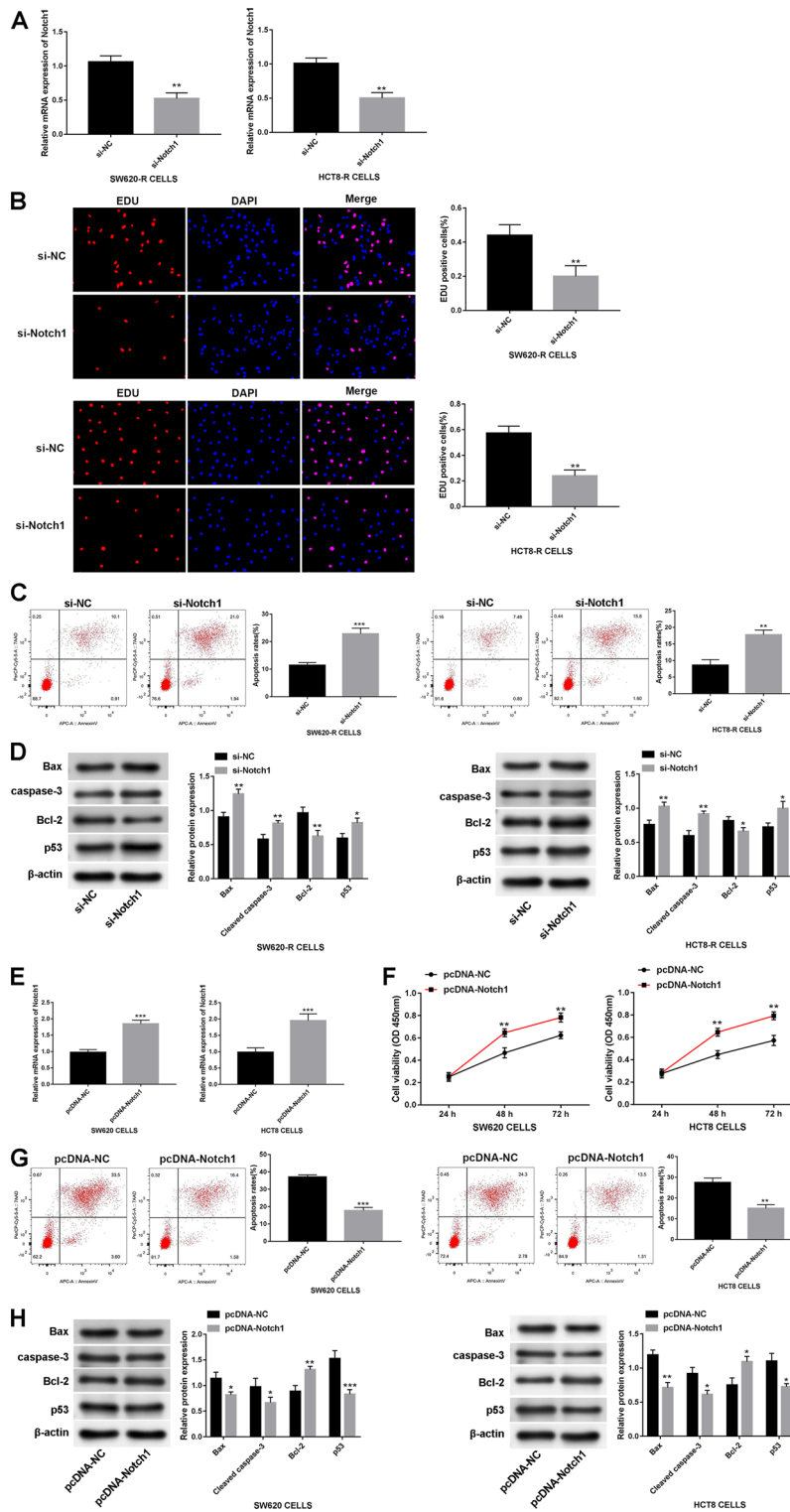


Fig. 2 (See legend on previous page.)

Notch1 affects the sensitivity of CRC cells to 5-FU and pyroptosis by regulating glycolysis

Drug-resistant cells often exhibit enhanced glycolysis; therefore, we evaluated glycolysis in SW620-R and HCT8-R cells. It turned out that SW620-R/HCT8-R cells' glucose level was obviously reduced relative to that in SW620/HCT8 cells ($P < 0.001$, Fig. 3A). Compared to SW620/HCT8 cells, expression levels of glucose transporter GLUTs (GLUT1, GLUT2, GLUT3, and GLUT4) in SW620-R/HCT8-R cells were determined, but only GLUT1 expression was significantly increased ($P < 0.001$, Fig. 3B). Meanwhile, the lactate level in SW620-R/HCT8-R cells was increased relative to that in SW620/HCT8 cells ($P < 0.01$, Fig. 3C). These results suggest that SW620-R/HCT8-R cells had increased glycolytic activity compared to SW620/HCT8 cells. Furthermore, we compared the viability of SW620-R/HCT8-R and SW620/HCT8 cells under conditions in which glycolysis was suppressed and cells were supplemented with lactate. We found that SW620-R/HCT8-R cells were more sensitive to glucose deficiency and lactate supplementation than SW620/HCT8 cells at the same concentration ($P < 0.05$, Fig. 3D, E). Next, we explored the effects of Notch1 on glycolysis in SW620-R and HCT8-R cells. Notch1 knockdown increased the glucose level in SW620-R and HCT8-R cells ($P < 0.01$, Fig. 3F). Notch1 knockdown reduced the lactate level in SW620-R and HCT8-R cells ($P < 0.01$, Fig. 3G).

It is previously illustrated that glycolysis-related protein PKM2 is a crucial rate-limiting enzyme participating in the Warburg effect, which bridges glycolysis and pyroptosis in microglia (Li et al. 2021; Su et al. 2023). In view of the intrinsic relation between glycolysis and pyroptosis, we next explored whether Notch1 made impact on pyroptosis of CRC cells by modulating glycolysis. Firstly, SW620-R and HCT8-R cells was treated with the competitive glycolysis inhibitor (2-DG, MedChemExpress) at a dose of 16 mmol/L for 24 h, and we detected the efficiency of 2-DG. We discovered that 2-DG markedly repressed glycolysis in SW620-R and HCT8-R cells, presenting as decreased GLUT1, LDHA, PKM2, PGK1, HK2, ALDOA ($P < 0.01$, Fig. 3H). Then rescue experiments were carried out. It was demonstrated that Notch1 overexpression evidently suppressed pyroptosis of SW620-R and HCT8-R cells, manifesting as decreased expression levels of pyroptosis-associated proteins (NLRP3, caspase-1, GSDMD-N, IL-18 and IL-1 β) ($P < 0.001$, Fig. 3I). However, the suppressive impact of Notch1 on pyroptosis was reversed by 2-DG ($P < 0.05$, Fig. 3I).

(See figure on next page.)

Fig. 3 Silencing of Notch1 improves 5-FU sensitivity of CRC cells promotes pyroptosis by inhibiting glycolysis. **A** A Glucose Assay Kit from Nanjing Jiancheng was used to assess the level of glucose in culture medium of SW620, SW620-R, HCT8 and HCT8-R cells. **B** Western blot was used to detect protein expression of GLUT1, GLUT2, GLUT3 and GLUT4 in SW620, SW620-R, HCT8 and HCT8-R cells. **C** A Lactate Assay Kit from Nanjing Jiancheng was applied to assess the level of lactate in culture medium of SW620, SW620-R, HCT8 and HCT8-R cells. **D** The viability of SW620, SW620-R, HCT8 and HCT8-R cells was detected CCK-8 assay after glucose treatment for 24 h. **E** The viability of SW620, SW620-R, HCT8 and HCT8-R cells was detected CCK-8 assay after lactate treatment for 24 h. **F** A Glucose Assay Kit from Nanjing Jiancheng was used to assess the level of glucose in culture medium of SW620-R and HCT8-R cells. **G** A Lactate Assay Kit from Nanjing Jiancheng was applied to assess the level of lactate in culture medium of SW620-R and HCT8-R cells. **H** Western blot was used to detect protein expression of GLUT1, LDHA, PKM2, PGK1, HK2, ALDOA in SW620-R and HCT8-R cells. **I** Western blot was used to detect protein expression of NLRP3, Caspase-1, GSDMD-N, IL-18 and IL-1 β in SW620-R and HCT8-R cells. * $P < 0.05$. ** $P < 0.01$. *** $P < 0.001$

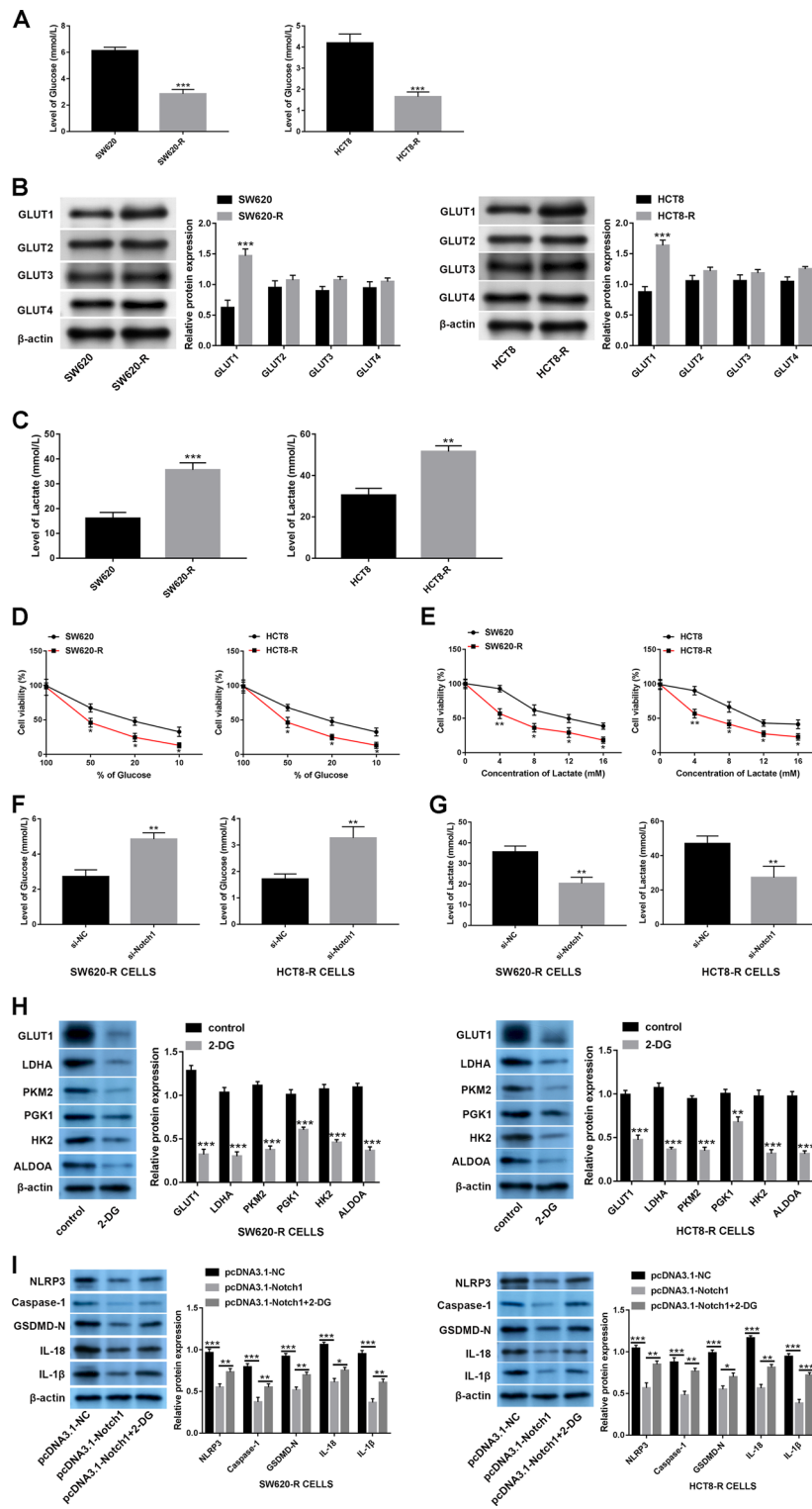


Fig. 3 (See legend on previous page.)

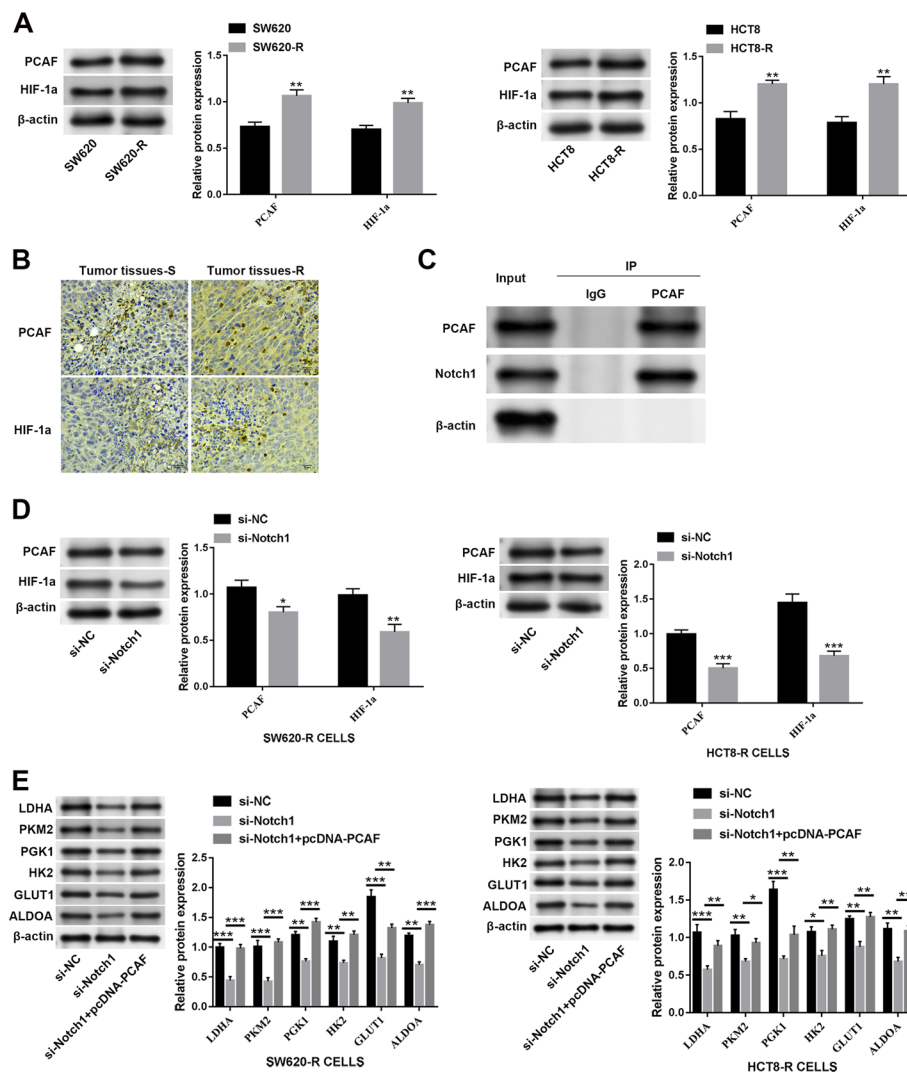


Fig. 4 Notch1 influences 5-FU resistance by PCAF/HIF-1 α -mediated glycolysis. **A** Western blot was used to detect protein expression of PCAF and HIF-1 α in SW620, SW620-R, HCT8 and HCT8-R cells. **B** Immunohistochemistry staining was used to detect protein expression of PCAF and HIF-1 α in sensitive tumor tissues and resistant tumor tissues from CRC patients. **C** Co-IP assay was used to examine direct interaction of PCAF and Notch1 in SW620-R cells. **D** Western blot was used to detect protein expression of PCAF and HIF-1 α in SW620-R and HCT8-R cells. **E** Western blot was used to detect protein expression of GLUT3, LDHA, PKM2, PGK1, HK2, GLUT1 and ALDOA in SW620-R and HCT8-R cells. * $P < 0.05$. ** $P < 0.01$. *** $P < 0.001$

Notch1 affects 5-FU resistance by PCAF/HIF-1 α -mediated glycolysis

PCAF interacts with HIF-1 α and affects cellular energy metabolism (Rajendran et al. 2013). To this end, we explored the expression of PCAF and HIF-1 α in 5-FU-resistant CRC cells and tissues. PCAF and HIF-1 α displayed higher protein expression in SW620-R/HCT8-R cells than in SW620/HCT8 cells ($P < 0.01$; Fig. 4A). Consistently, PCAF and HIF-1 α displayed higher protein expression levels in tumor tissues from 5-FU resistant CRC patients than in tissues from 5-FU sensitive CRC patients (Fig. 4B).

To determine whether Notch1 affects glycolysis by regulating the PCAF/HIF-1 α pathway, subsequent experiments were performed. According to the co-IP results, we observed a combination of PCAF and HIF-1 α in SW620-R cells, suggesting a direct

interaction between PCAF and HIF-1 α (Fig. 4C). Western blotting revealed that silencing Notch1 reduced PCAF and HIF-1 α expression levels in SW620-R and HCT8-R cells ($P < 0.05$, Fig. 4D). Moreover, we detected glycolysis-associated proteins, including GLUT3, LDHA, PKM2, PGK1, HK2, GLUT1, and ALDOA using western blotting. The protein levels of GLUT3, LDHA, PKM2, PGK1, HK2, GLUT1, and ALDOA were diminished after Notch1 down-regulation, and the suppressive effects of Notch1 down-regulation on these proteins were reversed by PCAF overexpression in SW620-R and HCT8-R cells ($P < 0.05$, Fig. 4E).

Synthesis and cellular uptake of PLAG NPs

This is a schematic diagram of PLGA NPs and si-Notch1 loading (Fig. 5A). The binding ability of PLGA to si-Notch1 was detected by agarose gel electrophoresis at different mass ratios. The ratio of PLGA NPs/si-Notch1 ranged from 0.125:1 to 16:1, resulting in decreased si-Notch1 mobility across the gel as the amount of PLGA NPs increased (Fig. 5B). There was no si-Notch1 band at 4:1, suggesting that the best ratio of PLGA NPs and si-Notch1. Then we also determined that the loading efficiency of PLGA NPs carrying si-Notch1/si-NC was $79.14 \pm 2.75\%$ and $80.29 \pm 3.78\%$, and the encapsulation efficiency of PLGA NPs containing si-Notch1/si-NC was $78.93 \pm 2.26\%$ and $76.42 \pm 1.08\%$. Moreover, we observed the shape of si-Notch1 supported by PLGA NPs (si-Notch1 PLGA NPs) using transmission electron microscope (TEM). TEM images showed that PLGA NPs and si-Notch1 PLGA NPs had a typical core-shell structure (Fig. 5C). According to DLS analysis, the particle sizes of PLGA NPs and si-Notch1 PLGA NPs were 96 ± 4.35 and 99 ± 1.28 nm (Fig. 5D). Meantime, The si-NC/si-Notch1 release study showed a 17% burst release on the first 1 day, followed by sustained release over 5 days (Fig. 5E). Then uptake of PLGA NPs with si-Notch1 cargo by SW620-R and HCT8-R cells was monitored using confocal microscopy. We discovered that PLGA NP/FAM-labeled si-Notch1 showed good internalization efficiency by SW620-R and HCT8-R cells when comparing lipo2000/FAM-labeled si-Notch1, as indicated by the green signals in the cytoplasm (Fig. 5F).

PLGA NPs-delivered si-Notch1 attenuates CRC cells' 5-FU resistance

To investigate the influence of PLGA NP-delivered si-Notch1 on 5-FU resistance in SW620-R and HCT8-R cells, the silencing efficiency of Notch1 was firstly assessed. As shown in Fig. 6A ($P < 0.001$), Notch1 expression in SW620-R and HCT8-R cells was dramatically reduced after si-Notch1 transfection with lipo2000 or PLGA NPs. SW620-R and HCT8-R cells transfected with si-Notch1 through lipo2000 or PLGA NPs were treated with 5-FU for 48 h to detect their viability and apoptosis. The viability of SW620-R and HCT8-R cells was reduced following si-Notch1 transfection with lipo2000 or PLGA NPs, and the PLGA NPs-si-Notch1 group showed the lowest cell viability compared with the other groups ($P < 0.01$, Fig. 6B). These results suggested that PLGA NPs-carried si-Notch1 synergistically enhance 5-FU-mediated cytotoxicity. In addition, the apoptosis rate in the PLGA NPs-si-Notch1 group was higher than that in the other groups ($P < 0.01$, Fig. 6C). Furthermore, we detected the IC₅₀ values after

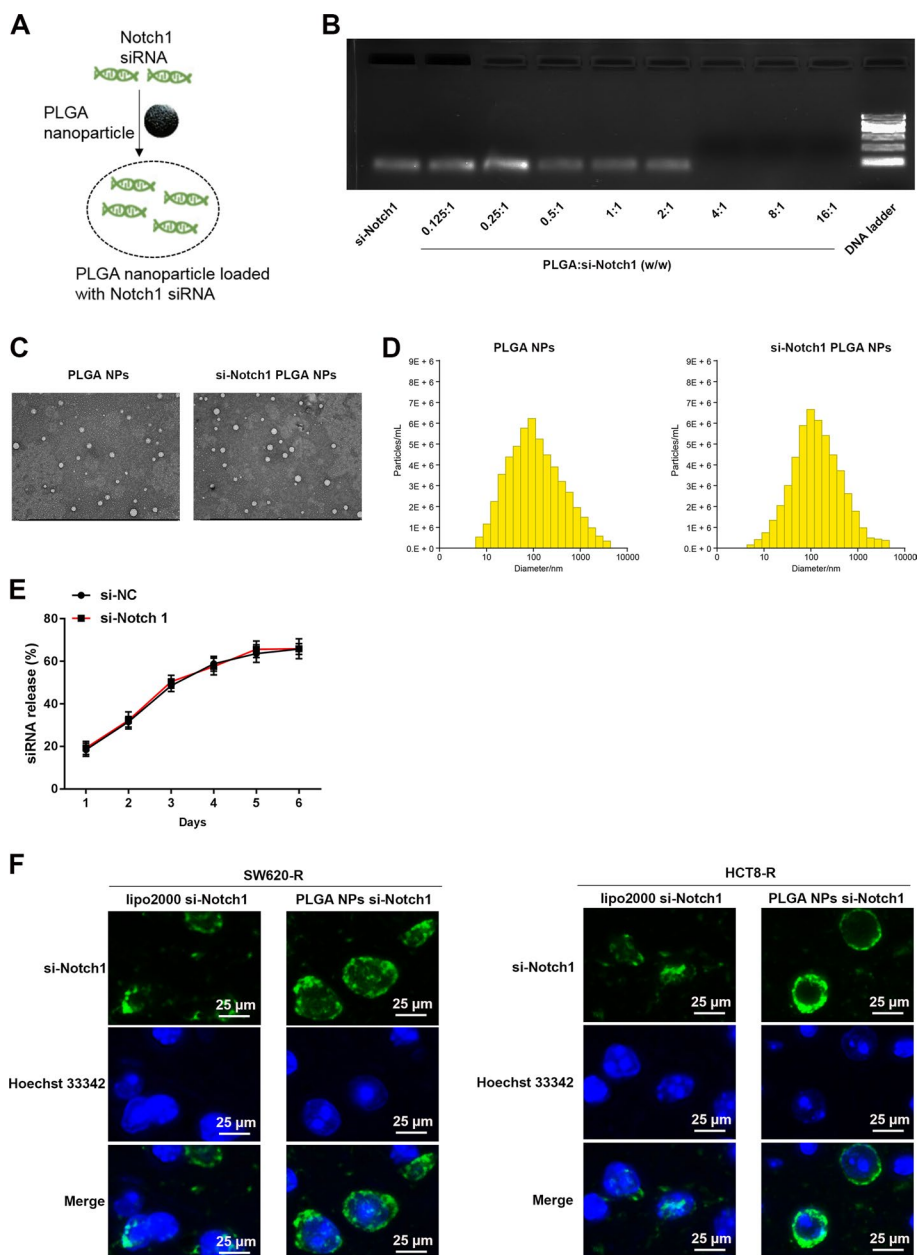


Fig. 5 Synthesis and cellular uptake of PLGA nanoparticles (NPs). **A** Sketch map showing synthesis of PLGA NPs and Notch1 siRNA loading. **B** The binding ability of PLGA NPs to Notch1 siRNA at different mass ratios was detected using agarose gel retardation electrophoresis. **C** Transmission electron microscope image showed the shape of the PLGA NPs. **D** Size distribution profiles of empty PLGA NPs and PLGA NPs containing Notch1 siRNA on DLS analysis. **E** In vitro release profile of siRNAs from siRNAs@PLGA NPs. **F** Confocal microscopic images of SW620-R and HCT8-R cells transfected with Notch1 siRNA using Lipofectamine 2000 or PLGA NPs. Green: fluorescein (FAM)-labeled siRNA; blue: Hoechst 33342-stained nuclei

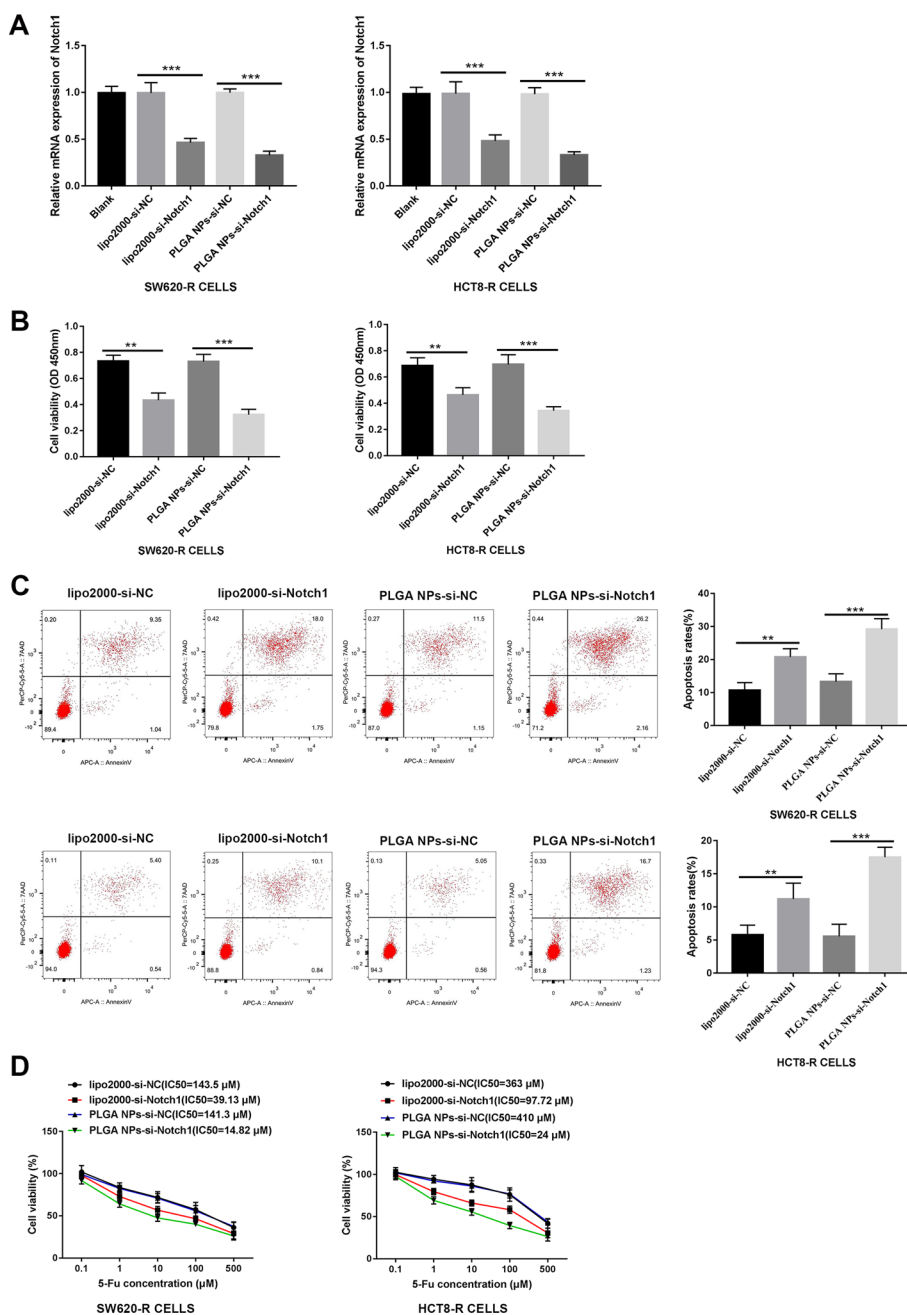


Fig. 6 PLGA NPs-delivered si-Notch1 reverses 5-FU resistance of CRC cells. **A** Relative expression of Notch1 in SW620-R and HCT8-R cells was detected by qRT-PCR. **B** The viability of SW620-R and HCT8-R cells was assessed by CCK-8 assay. **C** Apoptosis rates of SW620-R and HCT8-R cells were examined using flow cytometry analysis. **D** For calculate the half-maximal inhibitory concentration (IC50), the viability of SW620-R and HCT8-R cells was assessed by CCK-8 assay. ** $P < 0.01$. *** $P < 0.001$

SW620-R and HCT8-R cells were transfected with si-Notch1 using lipo2000 or PLGA NPs. We observed that the PLGA NPs-si-Notch1 group's IC50 value was lower than that of lipo2000-si-Notch1 (Fig. 6D). Based on these results, we deduced that the dose of 5-FU or siRNA could be decreased using PLGA NPs.

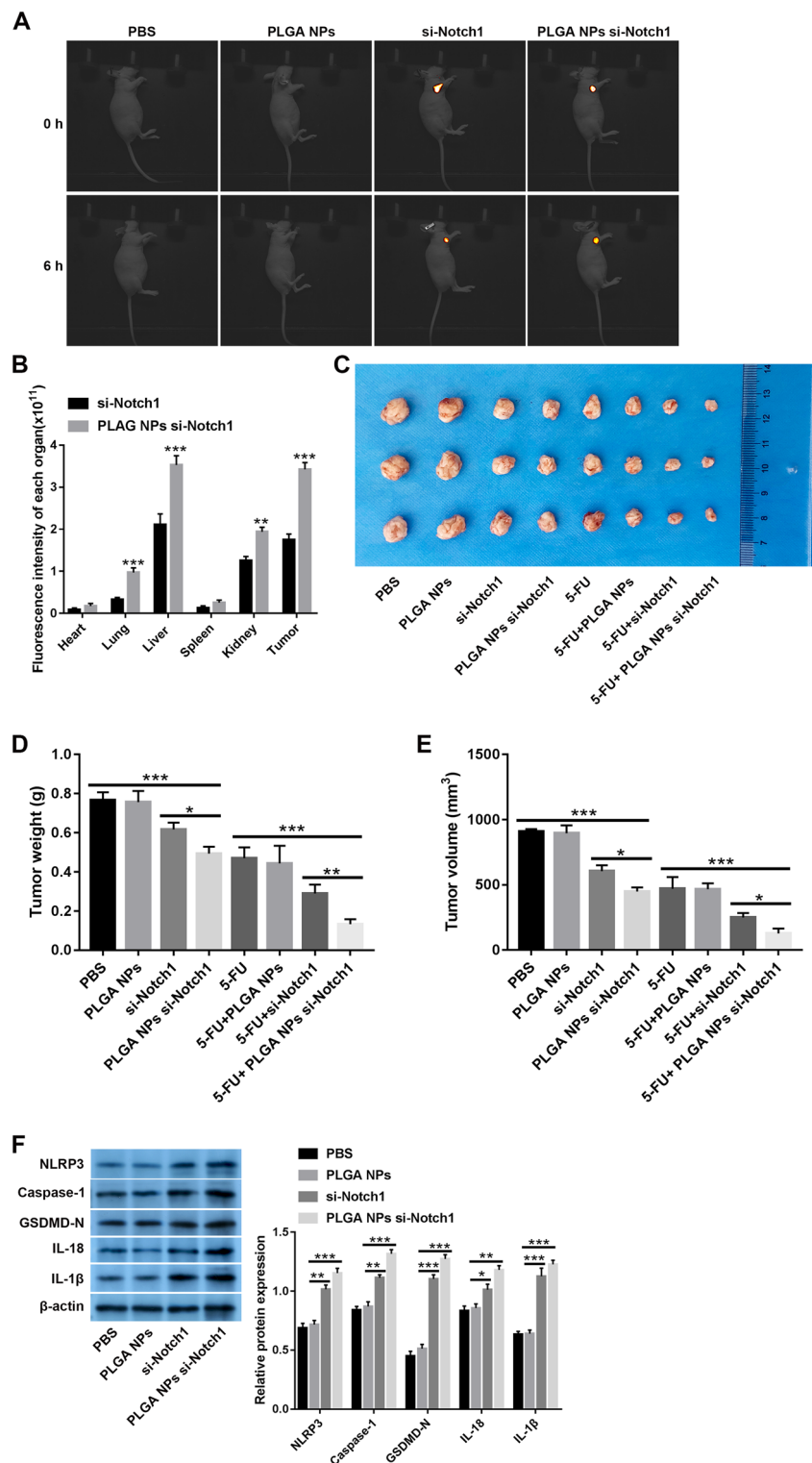


Fig. 7 PLGA NPs-mediated silencing of Notch1 enhances 5-FU toxicity in vivo. **A** In vivo imaging of xenograft-bearing mice after intra-tumoral injection of PBS, PLGA NPs, FAM-labeled si-Notch1, PLGA NPs containing FAM-labeled si-Notch1. **B** Biodistribution of FAM-labeled si-Notch1 and PLGA NPs containing FAM-labeled si-Notch1 in xenograft mice. **C** Images of the collected xenograft tumors. **D** Eventual tumor weight of xenograft mice. **E** Eventual tumor volume of xenograft mice. **F** Western blot was used to detect protein expression of NLRP3, Caspase-1, GSDMD-N, IL-18 and IL-1β in tumor tissues of mice. * $P < 0.05$. ** $P < 0.01$. *** $P < 0.001$

PLGA NPs-mediated silencing of Notch1 enhances 5-FU toxicity in vivo

Finally, we explored whether PLGA NP-delivered si-Notch1 could remain in tumors and reach cancer sites. We observed more intense fluorescence in tumor tissues in the PLGA NPs si-Notch1 group than in the si-Notch1 group (Fig. 7A). As shown in Fig. 7B, more accumulation of si-Notch1 was observed in the liver, lung, kidney and tumor of mice in the PLGA NPs si-Notch1 group than in those of the si-Notch1-only group ($P < 0.01$). This result suggested that the PLGA NPs si-Notch1 complex had favorable circulating stability, which was effectively delivered into tumor sites.

Besides, HCT8-R tumor-bearing mice were divided into PBS, PLGA NPs-only, si-Notch1-only, the PLGA NPs si-Notch1, 5-FU-only, 5-FU + PLGA NPs, 5-FU + si-Notch1, and 5-FU + PLGA NPs si-Notch1 group (Fig. 7C). We found that tumors in the PLGA NPs si-Notch1 group had lower tumor weight and smaller tumor volume compared to the si-Notch1-only group. Tumors in mice of the 5-FU + PLGA NPs si-Notch1 group had lower tumor weight and smaller tumor volume compared to the 5-FU + si-Notch1 group ($P < 0.05$, Fig. 7D, E). In addition, expression levels of pyroptosis-associated proteins (NLRP3, caspase-1, GSDMD-N, IL-18 and IL-1 β) were distinctly increased after introduction of si-Notch1 or PLGA NPs si-Notch1 in tumor tissues of mice ($P < 0.05$, Fig. 7F).

Discussion

In recent years, resistance to chemotherapy has remained a great challenge for CRC cure (Feng et al. 2021; Chen et al. 2022). Notch1 is responsible for drug resistance in laryngeal cancer, ovarian cancer and CRC (Li et al. 2022; Qian et al. 2020; Wang et al. 2016). Concurrently, convincing evidence has revealed that Notch1 expression is increased in sensitive CRC tissues and 5-FU-resistant CRC cells (Wang et al. 2022; Li et al. 2017; Liu et al. 2016). This expression trend of Notch1 was consistent with our findings, which also demonstrated the up-regulation of Notch1 expression in sensitive and resistant CRC tissues/cells. Furthermore, high Notch1 expression has been shown to be correlated with poor overall survival in CRC (Chu et al. 2010, 2011). Here, we also observed that patients with high Notch1 expression had shorter survival times than those with low Notch1 expression. These results suggested that Notch1 may be used as a novel prognostic biomarker for CRC. Above all, Notch1 is demonstrated to affect 5-FU resistance in CRC. For instance, silencing of Notch-1 facilitates the chemotherapeutic effect of 5-FU by regulating apoptosis in CRC cells (Liu et al. 2016). Down-regulation of lncRNA LINC00152 sensitizes CRC cells to 5-FU by reducing expression of Notch-1 (Bian et al. 2018). Similarly, our results indicated that knockdown of Notch1 reduced CRC cell resistance to 5-FU by suppressing cell proliferation and increasing apoptosis, confirming Notch-1 down-regulation's inhibitory effect on 5-FU resistance of CRC cells. Based on these findings, we deduced that agents targeting Notch-1 had the potential to manage tumor resistance to 5-FU in CRC patients.

It is well known that abnormal metabolism of cancer cells provides an environment that increases drug resistance and accelerates tumorigenesis (Montal et al. 2015). Many mechanisms of 5-FU resistance have been documented, such as changes in energy metabolism deregulation (Lohan-Codeco et al. 2022), 5-FU metabolic enzymes (Longley et al. 2003), drug influx or efflux rate (Mansoori et al. 2017) and the tumor

microenvironment (Gatenby et al. 2010). In this study, we explored the 5-FU resistance mechanism by which cancer cells affected glucose metabolism in CRC cells. SW620-R and HCT8-R cells showed higher glycolysis ability than sensitive SW620 and HCT8 cells, and Notch1 knockdown repressed glycolysis in SW620-R and HCT8-R cells. Similarly, the inhibitory effect of Notch1 knockdown on glycolysis is previously demonstrated in human mesenchymal stem cells under hypoxic conditions (Moriyama et al. 2014). Meantime, we found that Notch1 overexpression repressed pyroptosis of SW620-R and HCT8-R cells, which was reversed by glycolysis inhibitor. These findings suggested that Notch1 knockdown attenuated the resistance of CRC cells to 5-FU and promoted pyroptosis via suppressing glycolysis, offering a new molecular mechanism of Notch1 to affect CRC cells.

Taking into account the fact that PCAF can coordinate HIF-1 α and p53 to regulate energy metabolism in cancers (Rajendran et al. 2013; Xenaki et al. 2008), we speculated that the PCAF/HIF-1 α pathway was associated with glycolysis in CRC. Therefore, we expanded our investigation to probe whether PCAF/HIF-1 α was implicated in regulation of Notch1-mediated glycolysis. We found that expression levels of PCAF and HIF-1 α were markedly decreased after Notch1 knockdown in resistant CRC cells and tissues. Notch1 directly bound to PCAF. In particular, a reduction in levels of glycolysis-related proteins (GLUT3, LDHA, PKM2, PGK1, HK2, GLUT1, and ALDOA) in response to Notch1 knockdown was observed, which was reversed by PCAF overexpression in resistant CRC cells. Combining above findings, we inferred that the PCAF/HIF-1 α pathway was essential for Notch1-induced glycolysis. Our result was similar to a previous study, which has reported that Notch1 promotes glycolysis via functional interaction with PCAF in lung cancer (Xie et al. 2021).

PLGA polymers are considered delivery carriers for nucleotides and chemotherapeutics because of their biodegradability, retention effect, low cytotoxicity, and strong permeability in cancer treatment (Panyam and Labhasetwar 2003). Currently, some PLGA formulations are approved for drug delivery by the Food and Drug Administration (Perlstein et al. 2003; Acharya and Sahoo 2011). Therefore, PLGA NPs have drawn considerable attention as siRNA delivery vehicles for siRNA-mediated therapeutic applications. In our study, we used PLGA NPs to deliver si-Notch1 and to enhance Notch1 efficiency. Previous studies have demonstrated that the shape and small size of PLGA NPs are key factors for successful endocytosis of PLGA NPs (Muro et al. 2008). In particular, the size (<100 nm) of the NPs was more conducive to the encapsulation efficiency of siRNAs (Chithrani et al. 2006). We observed that PLGA NPs and si-Notch1 PLGA NPs had size homogeneity and displayed a typical core-shell structure. The size of the NP core in our study was approximately 96.0 or 99 nm, which is consistent with prior work (Chen et al. 2019). As expected, PLGA NPs-carried si-Notch1 displayed better-internalized efficiency by CRC cells than lipo2000-delivered si-Notch1 in vitro. When we tracked the in vivo bio-distribution of Cy5.5-siRNA PLGA NPs in mice, fluorescence exhibited strong Cy5.5 signals at the tumor sites, which indicated that siRNA@PLGA efficiently accumulated to tumor sites and showed good stability in vivo. Previously, PLGA NPs co-delivering si-MDR1 and si-BCL2 are reported to overcome resistance of paclitaxel and cisplatin in ovarian cancer (Risnayanti et al. 2018). In this study, we demonstrated that PLGA NPs co-delivering si-Notch1 significantly reduced 5-FU resistance in CRC

in vitro and in vivo. Taken together, we concluded that this delivery system was superior for drug release in CRC treatment, providing a novel and efficient delivery strategy to overcome the resistance of CRC cells.

Conclusions

In summary, high expression of Notch1 in sensitive or resistant CRC tissues/cells was observed, and Notch1 down-regulation sensitized CRC cells to 5-FU and promoted cell pyroptosis by regulating the PCAF/HIF-1 α pathway-mediated glycolysis. For the first time, we described a biomimetic drug delivery system (PLAG NPs) that was stable and effective for delivery of resistance reversal agents in CRC. Overall, our findings offer a promising option for the effective delivery of siRNA and precise therapy for CRC patients.

Abbreviations

siRNAs	Small interfering RNAs
CRC	Colorectal cancer
5-FU	The 5-fluorouracil-based
PPP	The pentose phosphate pathway

Supplementary Information

The online version contains supplementary material available at <https://doi.org/10.1186/s12645-024-00259-1>.

Additional file 1: Table S1. Association between Notch1 expression and clinical features of colorectal cancer patients.

Additional file 2: Figure S1. The expression of Notch1 in tumor tissues and adjacent normal tissues was analyzed using The Cancer Genome Atlas (TCGA) database.

Additional file 3: Figure S2. Correlation between Notch1 expression and overall survival of colorectal cancer patients was analyzed based on The Cancer Genome Atlas (TCGA) database.

Additional file 4: Figure S3. Relative mRNA expression of Notch1 detected by quantitative real-time polymerase chain reaction (qRT-PCR) in adjacent normal and tumor tissues of colorectal cancer patients.

Acknowledgements

Not applicable.

Author contributions

DDL, JCJ and TL designed the study. XWL and TL collected and analyzed the data. DDL and JCJ wrote the manuscript. SYL and FJJ made contributions in revising the manuscript. All authors read and approved the final manuscript.

Funding

This work was supported by the Beijing Medical Award Foundation (YXJL-2022-1906-0406, YXJL-2022-1906-0408, YXJL-2022-0436-0278), Norman Bethune Plan Program of Jilin University (2023B15), Jilin Province drug clinical rational use promotion project (Y202203), Natural Science Foundation of Jilin Provincial Department of Science and Technology-General program (YDZJ202201ZYTS011) and Natural Science Foundation of Jilin Provincial Department of Science and Technology-Discipline layout program (20210101274JC).

Availability of data and materials

All data generated or analyzed during this study are included in this published article and its supplementary information files.

Declarations

Ethics approval and consent to participate

This study was approved by the Ethics Committee of the China-Japan Union Hospital of Jilin University (2023-KYYS-021) and conformed to the Declaration of Helsinki. Written informed consent was obtained from all the enrolled patients. All experiments involving animals were approved by the Institutional Animal Care and Use Committee of the Jilin University (KT202302010). The experimental procedures were performed in accordance with the guidelines of the National Institute of Health.

Consent for publication

Not applicable.

Competing interests

The authors declare that they have no competing interests.

Received: 19 February 2024 Accepted: 29 March 2024

Published online: 12 April 2024

References

- Acharya S, Sahoo SK (2011) PLGA nanoparticles containing various anticancer agents and tumour delivery by EPR effect. *Adv Drug Deliv Rev* 63(3):170–183
- Arnold M, Sierra MS, Laversanne M, Soerjomataram I, Jemal A, Bray F (2017) Global patterns and trends in colorectal cancer incidence and mortality. *Gut* 66(4):683–691
- Bhattacharya B, Mohd Omar MF, Soong R (2016) The Warburg effect and drug resistance. *Br J Pharmacol* 173(6):970–979
- Bian Z, Zhang J, Li M, Feng Y, Yao S, Song M et al (2018) Correction: Long non-coding RNA LINC00152 promotes cell proliferation, metastasis, and confers 5-FU resistance in colorectal cancer by inhibiting miR-139-5p. *Oncogenesis* 7(8):63
- Bigas A, Martin DI, Milner LA (1998) Notch1 and Notch2 inhibit myeloid differentiation in response to different cytokines. *Mol Cell Biol* 18(4):2324–2333
- Biller LH, Schrag D (2021) Diagnosis and treatment of metastatic colorectal cancer: a review. *JAMA* 325(7):669–685
- Bray F, Ferlay J, Soerjomataram I, Siegel RL, Torre LA, Jemal A (2018) Global cancer statistics 2018: GLOBOCAN estimates of incidence and mortality worldwide for 36 cancers in 185 countries. *CA Cancer J Clin* 68(6):394–424
- Cartiera MS, Johnson KM, Rajendran V, Caplan MJ, Saltzman WM (2009) The uptake and intracellular fate of PLGA nanoparticles in epithelial cells. *Biomaterials* 30(14):2790–2798
- Chen M, Chen M, He J (2019) Cancer cell membrane cloaking nanoparticles for targeted co-delivery of doxorubicin and PD-L1 siRNA. *Artif Cells Nanomed Biotechnol* 47(1):1635–1641
- Chen G, Gong T, Wang Z, Wang Z, Lin X, Chen S et al (2022) Colorectal cancer organoid models uncover oxaliplatin-resistant mechanisms at single cell resolution. *Cell Oncol* 45(6):1155–1167
- Chithrani BD, Ghazani AA, Chan WC (2006) Determining the size and shape dependence of gold nanoparticle uptake into mammalian cells. *Nano Lett* 6(4):662–668
- Chu D, Li Y, Wang W, Zhao Q, Li J, Lu Y et al (2010) High level of Notch1 protein is associated with poor overall survival in colorectal cancer. *Ann Surg Oncol* 17(5):1337–1342
- Chu D, Zhou Y, Zhang Z, Li Y, Li J, Zheng J et al (2011) Notch1 expression, which is related to p65 Status, is an independent predictor of prognosis in colorectal cancer. *Clin Cancer Res* 17(17):5686–5694
- Davidson BL, McCray PB Jr (2011) Current prospects for RNA interference-based therapies. *Nat Rev Genet* 12(5):329–340
- DeBerardinis RJ, Chandel NS (2016) Fundamentals of cancer metabolism. *Sci Adv* 2(5):e1600200
- DeBerardinis RJ, Lum JJ, Hatzivassiliou G, Thompson CB (2008) The biology of cancer: metabolic reprogramming fuels cell growth and proliferation. *Cell Metab* 7(1):11–20
- Diaz-Ruiz R, Rigoulet M, Devin A (2011) The Warburg and Crabtree effects: on the origin of cancer cell energy metabolism and of yeast glucose repression. *Biochem Biophys Acta* 1807(6):568–576
- Dong S, Liang S, Cheng Z, Zhang X, Luo L, Li L et al (2022) ROS/PI3K/Akt and Wnt/beta-catenin signalings activate HIF-1alpha-induced metabolic reprogramming to impart 5-fluorouracil resistance in colorectal cancer. *J Exp Clin Cancer Res* CR 41(1):15
- Du Y, Li D, Li N, Su C, Yang C, Lin C et al (2018) POFUT1 promotes colorectal cancer development through the activation of Notch1 signaling. *Cell Death Dis* 9(10):995
- Fang Y, Tian S, Pan Y, Li W, Wang Q, Tang Y et al (2020) Pyroptosis: a new frontier in cancer. *Biomed Pharmacother Biomed Pharmacother* 121:109595
- Feng M, Zhao Z, Yang M, Ji J, Zhu D (2021) T-cell-based immunotherapy in colorectal cancer. *Cancer Lett* 498:201–209
- Firouzi-Amandi A, Dadashpour M, Nouri M, Zarghami N, Serati-Nouri H, Jafari-Gharabaghlu D et al (2018) Chrysin-nanoencapsulated PLGA-PEG for macrophage repolarization: Possible application in tissue regeneration. *Biomed Pharmacother Biomed Pharmacother* 105:773–780
- Gatenby RA, Gillies RJ, Brown JS (2010) Evolutionary dynamics of cancer prevention. *Nat Rev Cancer* 10(8):526–527
- Ghareghomi S, Ahmadian S, Zarghami N, Hemmati S (2021) hTERT-molecular targeted therapy of ovarian cancer cells via folate-functionalized PLGA nanoparticles co-loaded with MNPs/siRNA/wortmannin. *Life Sci* 277:119621
- Grothey A, Sobrero AF, Shields AF, Yoshino T, Paul J, Taieb J et al (2018) Duration of adjuvant chemotherapy for stage III colon cancer. *N Engl J Med* 378(13):1177–1188
- Hagan S, Orr MC, Doyle B (2013) Targeted therapies in colorectal cancer—an integrative view by PPPM. *EPMA J* 4(1):3
- Hay N (2016) Reprogramming glucose metabolism in cancer: can it be exploited for cancer therapy? *Nat Rev Cancer* 16(10):635–649
- Kanasty RL, Whitehead KA, Vegas AJ, Anderson DG (2012) Action and reaction: the biological response to siRNA and its delivery vehicles. *Mol Ther J Am Soc Gene Ther* 20(3):513–524
- Kim J, Kang J, Kang YL, Woo J, Kim Y, Huh J et al (2020) Ketohexokinase-A acts as a nuclear protein kinase that mediates fructose-induced metastasis in breast cancer. *Nat Commun* 11(1):5436
- Leong KG, Gao WQ (2008) The Notch pathway in prostate development and cancer. *Diff Res Biol Ity* 76(6):699–716
- Li G, Zhou Z, Zhou H, Zhao L, Chen D, Chen H et al (2017) The expression profile and clinicopathological significance of Notch1 in patients with colorectal cancer: a meta-analysis. *Future Oncol* 13(23):2103–2118

- Li M, Lu H, Wang X, Duan C, Zhu X, Zhang Y et al (2021) Pyruvate kinase M2 (PKM2) interacts with activating transcription factor 2 (ATF2) to bridge glycolysis and pyroptosis in microglia. *Mol Immunol* 140:250–266
- Li D, Xu D, Chen P, Xie J (2022) Notch1 signaling modulates hypoxia-induced multidrug resistance in human laryngeal cancer cells. *Mol Biol Rep* 49(7):6235–6240
- Liu H, Yin Y, Hu Y, Feng Y, Bian Z, Yao S et al (2016) miR-139-5p sensitizes colorectal cancer cells to 5-fluorouracil by targeting NOTCH-1. *Pathol Res Pract* 212(7):643–649
- Lohan-Codeco M, Barambo-Wagner ML, Nasciutti LE, Ribeiro Pinto LF, Meireles Da Costa N, Palumbo A Jr (2022) Molecular mechanisms with chemoresistance in esophageal cancer. *Cell Mol Life Sci CMLS* 79(2):116
- Longley DB, Harkin DP, Johnston PG (2003) 5-fluorouracil: mechanisms of action and clinical strategies. *Nat Rev Cancer* 3(5):330–338
- Luk BT, Hu CM, Fang RH, Dehaini D, Carpenter C, Gao W et al (2014) Interfacial interactions between natural RBC membranes and synthetic polymeric nanoparticles. *Nanoscale* 6(5):2730–2737
- Mansoori B, Mohammadi A, Davudian S, Shirjang S, Baradaran B (2017) The different mechanisms of cancer drug resistance: a brief review. *Adv Pharm Bull* 7(3):339–348
- Mohammad Gholinia Sarpoli L, Zare-Karizi S, Heidari E, Hasanzadeh A, Bayandori M, Azedi F et al (2022) Co-delivery of curcumin and Bcl-2 siRNA to enhance therapeutic effect against breast cancer cells using PEI-functionalized PLGA nanoparticles. *Pharm Dev Technol* 27(7):785–793
- Montal ED, Dewi R, Bhalla K, Ou L, Hwang BJ, Ropell AE et al (2015) PEPCK coordinates the regulation of central carbon metabolism to promote cancer cell growth. *Mol Cell* 60(4):571–583
- Moriyama H, Moriyama M, Isshi H, Ishihara S, Okura H, Ichinose A et al (2014) Role of notch signaling in the maintenance of human mesenchymal stem cells under hypoxic conditions. *Stem Cells Dev* 23(18):2211–2224
- Muro S, Garnacho C, Champion JA, Leferovich J, Gajewski C, Schuchman EH et al (2008) Control of endothelial targeting and intracellular delivery of therapeutic enzymes by modulating the size and shape of ICAM-1-targeted carriers. *Mol Ther J Am Soc Gene Ther* 16(8):1450–1458
- Najahi-Missaoui W, Arnold RD, Cummings BS (2020) Safe nanoparticles: are we there yet? *Int J Mol Sci* 22(1):385
- Nicolas M, Wolfer A, Raj K, Kummer JA, Mill P, van Noort M et al (2003) Notch1 functions as a tumor suppressor in mouse skin. *Nat Genet* 33(3):416–421
- Panyam J, Labhasetwar V (2003) Biodegradable nanoparticles for drug and gene delivery to cells and tissue. *Adv Drug Deliv Rev* 55(3):329–347
- Pavlova NN, Thompson CB (2016) The emerging hallmarks of cancer metabolism. *Cell Metab* 23(1):27–47
- Perlstein I, Connolly JM, Cui X, Song C, Li Q, Jones PL et al (2003) DNA delivery from an intravascular stent with a denatured collagen-poly(lactide-co-glycolic acid)-controlled release coating: mechanisms of enhanced transfection. *Gene Ther* 10(17):1420–1428
- Pho-lam T, Punnakitkashem P, Somboonyosdech C, Sripinitchai S, Masaratana P, Sirivatanauksorn V et al (2021) PLGA nanoparticles containing alpha-fetoprotein siRNA induce apoptosis and enhance the cytotoxic effects of doxorubicin in human liver cancer cell line. *Biochem Biophys Res Commun* 553:191–197
- Qian XQ, Tang SS, Shen YM, Chen LL, Cheng XD, Wan XY (2020) Notch1 affects chemo-resistance through regulating epithelial-mesenchymal transition (EMT) in epithelial ovarian cancer cells. *Int J Med Sci* 17(9):1215–1223
- Rajendran R, Garva R, Ashour H, Leung T, Stratford I, Krstic-Demonacos M et al (2013) Acetylation mediated by the p300/CBP-associated factor determines cellular energy metabolic pathways in cancer. *Int J Oncol* 42(6):1961–1972
- Risnayani C, Jang YS, Lee J, Ahn HJ (2018) PLGA nanoparticles co-delivering MDR1 and BCL2 siRNA for overcoming resistance of paclitaxel and cisplatin in recurrent or advanced ovarian cancer. *Sci Rep* 8(1):7498
- Sadat Tabatabaei Mirakabad F, Nejati-Koshki K, Akbarzadeh A, Yamchi MR, Milani M, Zarghami N et al (2014) PLGA-based nanoparticles as cancer drug delivery systems. *Asian Pac J Cancer Prev APJCP* 15(2):517–535
- Semenza GL (2002) HIF-1 and tumor progression: pathophysiology and therapeutics. *Trends Mol Med* 8(4 Suppl):S62–S67
- Semenza GL (2003) Targeting HIF-1 for cancer therapy. *Nat Rev Cancer* 3(10):721–732
- Setten RL, Rossi JJ, Han SP (2019) The current state and future directions of RNAi-based therapeutics. *Nat Rev Drug Discov* 18(6):421–446
- Shen J, Li M (2018) MicroRNA-744 inhibits cellular proliferation and invasion of colorectal cancer by directly targeting onco-gene Notch1. *Oncol Res* 26(9):1401–1409
- Singh A, Trivedi P, Jain NK (2018) Advances in siRNA delivery in cancer therapy. *Artif Cells Nanomed Biotechnol* 46(2):274–283
- Su P, Mao X, Ma J, Huang L, Yu L, Tang S et al (2023) ERRalpha promotes glycolytic metabolism and targets the NLRP3/caspase-1/GSDMD pathway to regulate pyroptosis in endometrial cancer. *J Exp Clin Cancer Res* 42(1):274
- Thorne JL, Campbell MJ, Turner BM (2009) Transcription factors, chromatin and cancer. *Int J Biochem Cell Biol* 41(1):164–175
- Tyagi A, Sharma AK, Damodaran C (2020) A review on notch signaling and colorectal cancer. *Cells* 9(6):1549
- Vinson KE, George DC, Fender AW, Bertrand FE, Sigounas G (2016) The Notch pathway in colorectal cancer. *Int J Cancer* 138(8):1835–1842
- Wallberg AE, Pedersen K, Lendahl U, Roeder RG (2002) p300 and PCAF act cooperatively to mediate transcriptional activation from chromatin templates by notch intracellular domains in vitro. *Mol Cell Biol* 22(22):7812–7819
- Wang Y, Liu Y, Tang F, Bernot KM, Schore R, Marcucci G et al (2014) Echinomycin protects mice against relapsed acute myeloid leukemia without adverse effect on hematopoietic stem cells. *Blood* 124(7):1127–1135
- Wang R, Ye X, Bhattacharya R, Boulbes DR, Fan F, Xia L et al (2016) A disintegrin and metalloproteinase domain 17 regulates colorectal cancer stem cells and chemosensitivity via Notch1 signaling. *Stem Cells Transl Med* 5(3):331–338
- Wang J, Sun M, Ma R, Wang G, Li W, Yang B et al (2022) Down-regulation of NOTCH1 and PKM2 can inhibit the growth and metastasis of colorectal cancer cells. *Am J Transl Res* 14(8):5455–5465
- Xenaki G, Ontikatzte T, Rajendran R, Stratford IJ, Dive C, Krstic-Demonacos M et al (2008) PCAF is an HIF-1alpha cofactor that regulates p53 transcriptional activity in hypoxia. *Oncogene* 27(44):5785–5796
- Xie M, Fu XG, Jiang K (2021) Notch1/TAZ axis promotes aerobic glycolysis and immune escape in lung cancer. *Cell Death Dis* 12(9):832

- Yang F, Bettadapura SN, Smeltzer MS, Zhu H, Wang S (2022) Pyroptosis and pyroptosis-inducing cancer drugs. *Acta Pharmacol Sin* 43(10):2462–2473
- Zhang N, Yin Y, Xu SJ, Chen WS (2008) 5-Fluorouracil: mechanisms of resistance and reversal strategies. *Molecules* 13(8):1551–1569
- Zhao J, Xiao A, Liu C, Ye C, Yin K, Lu M et al (2020) The HIF-1A/miR-17-5p/PDCD4 axis contributes to the tumor growth and metastasis of gastric cancer. *Signal Transduct Target Ther* 5(1):46

Publisher's Note

Springer Nature remains neutral with regard to jurisdictional claims in published maps and institutional affiliations.